PAPER

The transport properties in graphene/single-unit-cell cuprates van der Waals heterostructure

IOP ebooks™

Bringing you innovative digital publishing with leading voices to create your essential collection of books in STEM research.

Start exploring the collection - download the first chapter of every title for free.

The transport properties in graphene/single-unit-cell cuprates van der Waals heterostructure

HPSTAR
785-2019

Yufeng Wu[1,3,4], Hong Xiao[2] , Qiao Li[1,3], Xiaojiang Li[1,3], Zhuojun Li[1,3],
Gang Mu[1,3], Da Jiang[1,3], T Hu[1,3,5] and X M Xie[1,3,4]

[1] State Key Laboratory of Functional Materials for Informatics, Shanghai Institute of Microsystem and Information Technology, Chinese Academy of Sciences, Shanghai 200050, People's Republic of China
[2] Center for High Pressure Science and Technology Advanced Research, Beijing, 100094, People's Republic of China
[3] CAS Center for Excellence in Superconducting Electronics(CENSE), Shanghai 200050, People's Republic of China
[4] University of Chinese Academy of Science, Beijing 100049, People's Republic of China

E-mail: jiangda@mail.sim.ac.cn and thu@mail.sim.ac.cn

CrossMark

Abstract

Inducing superconductivity into graphene by a proximity effect offers a chance to study exotic physics phenomena involved in Cooper pairs on a Dirac fermions system. Here we fabricate the monolayer graphene/single-unit-cell $Bi_2Sr_2CaCu_2O_{8+x}$ (single-unit-cell Bi2212) van der Waals heterostructure, where the atomically flat surface from mechanically exfoliated single-unit-cell Bi2212 is the key to the pronounced proximity effect. The transport measurements in combination with direct and alternating current are performed on graphene/single-unit-cell Bi2212. The superconductivity is observed at the graphene/single-unit-cell Bi2212 heterostructure below 86 K. In the superconducting state, the nonlinear drain current–voltage relation is seen reflecting the characterisation of the Dirac–fermionic band structure of graphene. While for a lower bias, the differential conductance spectra shows a small subgap up to 60 K, implying a proximity-induced high-temperature superconductivity in graphene. Our results open a new way to study the superconductivity in two-dimensional Dirac fermion systems.

Keywords: graphene, superconductivity, Bi2212, van der Waals, single unit cell, heterojunction

(Some figures may appear in colour only in the online journal)

1. Introduction

Graphene at one-atom thick has attracted a lot of interest because of its wonderful properties, such as superior mechanical strength, high carrier mobility, high electrical and thermal conductivity, chemically inert properties and the linear dispersive electronic structure [1–6]. Recent research on graphene has gotten involved in the combination of graphene with superconductivity. Graphene becomes superconducting by coupling with the twisted graphene underneath [7] or by proximity effect in superconductor–graphene–

superconductor junctions [8–12], superconducting nanoislands on graphene [13–16], superconductor–graphene heterostructures [17–19] and so on. Amongst them, the superconductor–graphene heterostructure provides a relatively easy way [20, 21] to study proximity-induced superconductivity in the two-dimensional relativistic electronic system of graphene.

Superconducting proximity effect occurs when a normal metal is brought into contact with a superconductor. The Cooper pairs penetrate from the superconductor (S) into an adjacent non-superconducting metal (N). The microscopic mechanism describing superconducting proximity effect is Andreev reflection (AR). It describes how an electron on

---

[5] Author to whom any correspondence should be addressed.

normal metal at energies less than the superconducting energy gap is reflected as a hole with opposite spin and velocity but equal momentum by an adjacent superconductor, meanwhile a Cooper pair is created in the superconductor [22]. In contrast to normal metal, graphene is proposed to experience the specular Andreev reflection, where the *AR* related electron and hole lie in different valleys of the band structure [20, 21]. Up to now, most of the previous works on proximity effect in graphene were carried out based on the low-temperature superconductor. In contrast, graphene in proximity contact with a high-temperature cuprate superconductor demonstrate spectral features: e.g. proximity-induced *p*–wave super-conductivity in graphene/$Pr_{2-x}Ce_xCuO_4$ (PCCO) hetero-structure [19]; Klein-like tunnelling of high-temperature superconducting pairs in graphene/$YBa_2Cu_3O_7$ (YBCO) structure [23]. In our previous work, the graphene/cuprates van der Waals heterostructures were achieved by assembling graphene with the exfoliated-cuprate superconductor $Bi_2Sr_2CaCu_2O_{8+x}$ (Bi2212) [18]. In the heterostructures, it is found that the superconductivity even for single-unit-cell Bi2212 can persist up to 88 K [18], which is much higher than that of an electron-doped cuprate. In addition, graphene-cuprates structures is the van der Waals heterostructure which has a more clean and sharper interfaces because the van der Waals forces can push trapped contaminants into micrometer size bubbles [24]. Thus, the graphene/cuprates van der Waals heterostructure is the best candidate to the proximity-induced high-temperature superconductivity and the associated physics phenomena in graphene.

In this paper, we fabricate the monolayer graphene/single-unit-cell Bi2212 van der Waals heterostructure by dry transfer of monolayer graphene onto mechanically exfoliated Bi2212. A combination of direct current (DC) and alternating current transport measurements are performed in this heterostructure. Under large bias current (voltage), we find that the heterostructure demonstrates the nonlinear drain current–voltage behavior which reflects the linear dispersion of massless Dirac fermions in graphene. While at the small bias, a small subgap is observable in the superconducting state up to 60 K implying a proximity-induced superconducting gap.

2. Experiment

2.1. The structure of graphene/single-unit-cell Bi2212

The heterostructure was fabricated by the previously developed transfer technique as shown in figure 1(a) [18]. The monolayer graphene is a continuous film grown by chemical vapor deposition method on the Cu foil [25]. The as-grown graphene is covered with a layer of spin-coated PMMA and cured in O_2/Ar (20 s.c.c.m./200 s.c.c.m.) at 200 °C for about 30 min for better contacts. The Cu substrate (Alfa Aesar) was then dissolved by an aqueous solution of ferric chloride (0.1 g/mL) and the PMMA-graphene is then washed with deionized water and dried on the quartz substrate. After that, we exfoliate the single-unit-cell Bi2212 on the quartz substrate by scotch tape. Immediately after the Bi2212 flakes are
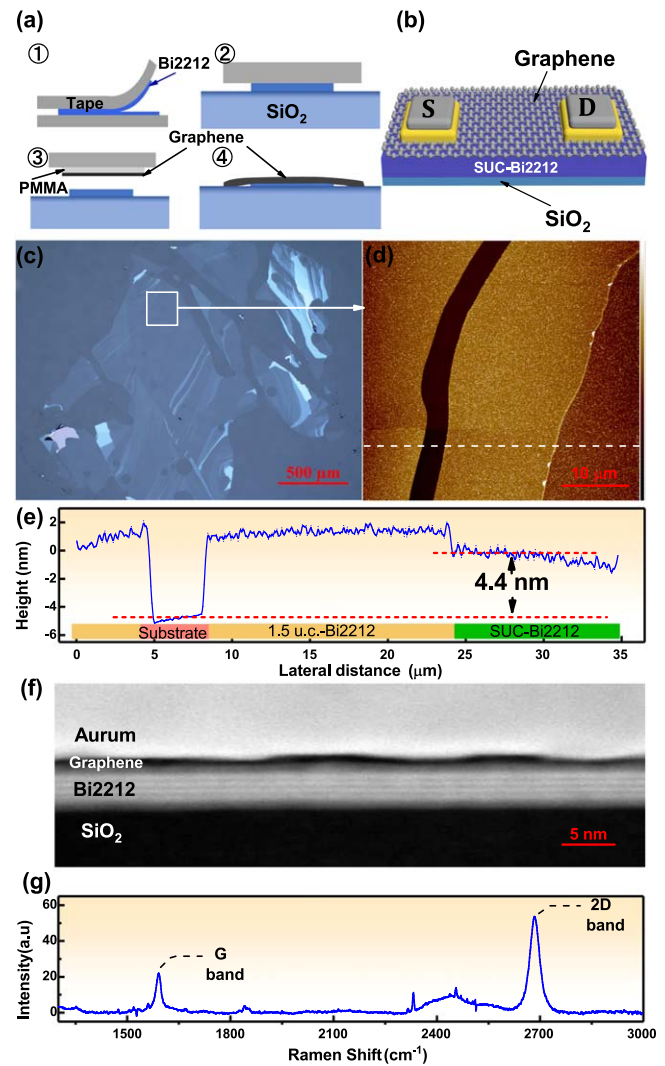

Figure 1. (a) The fabrication process of the monolayer graphene/single-unit-cell Bi2212 van der Waals heterostructures [18]. (b) Schematic plot of the device. (c) Optical microscope images. The thick Bi2212 is white, the single-unit-cell Bi2212 is light blue and the quartz substrate is blue. (d) Atomic force microscope (*AFM*) image of the sample from the square in (c). (e) The measured height from *AFM* in (d): From left to right, the single-unit-cell Bi2212 is brown, the thick Bi2212 is yellow and the quartz is dark brown. (f) Transmission electron microscope (TEM) image of the sample cross section: From top to bottom. The uppermost gold is white, the middle graphene is black, the next Bi2212 is white stripe, and the bottommost substrate is black. (g) Raman spectroscopy of the heterostructure. The *G* and 2*D* band peaks for the graphene are marked with dashed lines.

fabricated, the prepared tape-PMMA-graphene is transferred onto the top of the Bi2212 flakes. To get ride of the PMMA film on the heterostructure, the PMMA was dissolved by acetone. The freshly cleaved surfaces of graphene and the Bi2212 layer are contacted through the van der Waals force. Figure 1(b) is the configuration of the transport measurement for the graphene/single-unit-cell Bi2212 device.

Figure 1(c) is the metallographic microscope picture of the fabricated monolayer graphene/single-unit-cell Bi2212 van der Waals heterostructure. The thickness of different regions of the sample can be distinguished by the color in the

metallographic microscope picture due to the interference shift. The thick Bi2212 flake shows white color, while the thinnest or the single-unit cell Bi2212 (single-unit-cell Bi2212) flakes look blue color as the square region in the figure 1(c). Figure 1(d) is atomic force microscope (*AFM*) image for the sample in the square region of figure 1(c). The thickness of the Bi2212 flakes is also determined by the *AFM* from figure 1(e), where the measured step height is about 4 nm which is slightly larger than the actual value of single-unit cell Bi2212 (3nm). Considering the influence of the chemical contrast and the gap between the flake and the substrate, the value of 4 nm indeed confirms that this Bi2212 flake is single-unit cell thick. Figure 1(f) is the transmission electron microscope (TEM) image of the cross section of the heterostructure. Through the clear boundary, the entire Bi2212 sample shows very uniform thickness of about 4 nm. It can also be seen that the interface between graphene and Bi2212 as well as gold remains intact even after transfer processes and the deposition of gold. In addition, Raman spectroscopy was carried out on the heterostructure as shown in figure 1(g). The 2*D* band peak (2686 cm^{-1}) is much larger than *G* band peak (1590 cm^{-1}) confirming that the graphene on the Bi2212 is a monolayer. The *D* band (about 1350 cm^{-1}) is almost covered up, suggesting the monolayer graphene contains fewer defects but still has relatively good quality.

2.2. Electrical transport measurement of graphene/single-unit-cell Bi2212

Figure 2(a) is the DC drain current–voltage ($I − V$) curves of graphene/single-unit-cell Bi2212 heterostructure measured at the temperature (T) between 5 K and 90 K and zero magnetic field by electrical transport options in the physical property measurement system (PPMS) from Quantum Design. The schematic plot of the measurement configuration is shown in the bottom inset to figure 2(b). Inset to figure 2(a) is the temperature (T) dependence of the differential resistance (dV/dI) measured at zero bias. The dV/dI shows a sharp drop at 86 K and a following slow increase as cooling down. Such a non-monotonic temperature dependent dV/dI behavior is known as 'reentrance effect' [26, 27] and widely observed in normal metal-superconductor junction at very low temperature and small bias voltage [28, 29]. This reentrance effect is due to nonequilibrium effects between electron pairs leaking from superconductor and quasiparticles injected by the normal metal. [26, 30]. Actually, the resistance of a thin normal metal in the presence of proximity-induced superconducting correlations will not vanish, since the proximity-induced superconductivity of non-interacting electrons differs from true superconductivity of electrons [30, 31]. The physics behind the non-vanish resistance is that Andreev reflection spoils the time-reversing properties [32], which is also responsible a non-zero voltage value at a bias current below the superconducting state. The value of T_c is consistent with the previous report for single-unit-cell Bi2212 [18]. Above the T_c, the V increases almost linearly with the increase of I as shown in the main plot of figure 2(a). While below T_c, the V demonstrates a significant nonlinear behavior. It increases
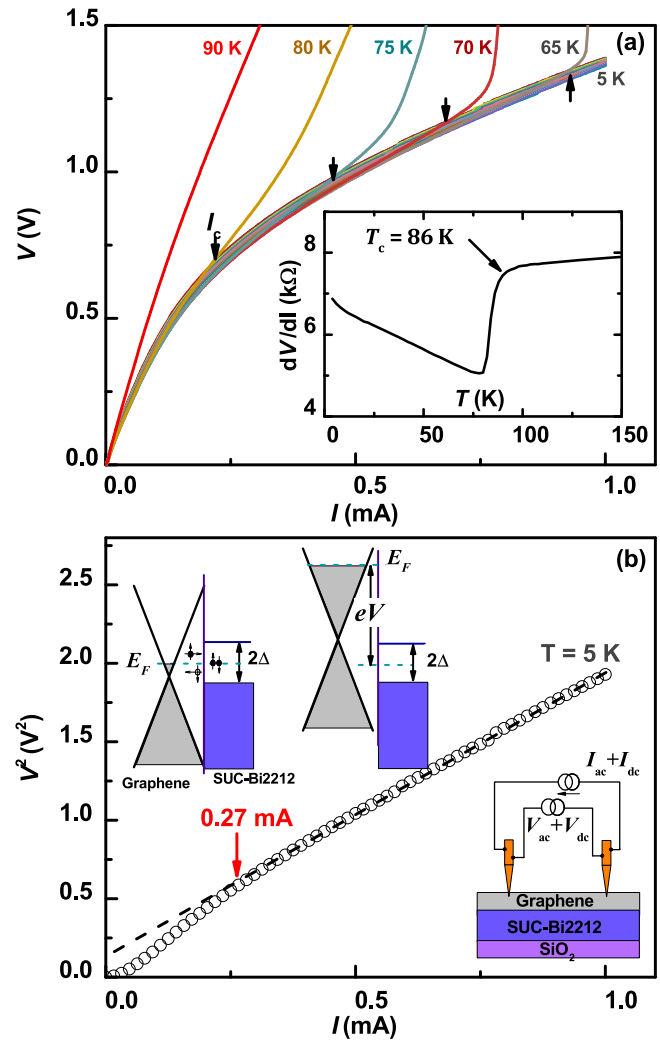

Figure 2. (a) The current (I) dependence of drain-source voltage (V) for the graphene/single-unit-cell Bi2212 heterostructure device at the temperature range 5 K $\leqslant T \leqslant$ 90 K. The inset: dV/dI v.s. T at zero bias. The dash arrow marks the T_c of Bi2212. (b) $I − V^2$ curve. The dashed line is the linear fitting above $I = 0.27$ mA (the red arrow). The top inset: schematic illustration of two tunneling mechanisms. left: $|E_F| \sim |\Delta|$. right: $|E_F| \gg |\Delta|$, where E_F is the Fermi level of graphene and Δ is the superconducting gap of single-unit-cell Bi2212. The bottom inset: the circuit configuration of the device.

with the increase of current and shows an abrupt upturn at the critical current (I_c).

3. Discussion

The I_c (the arrows in figure 2(a)) increases as cooling down begins, which can be understood as the superconducting critical current. Thus the superconductivity of the single-unit-cell Bi2212 is suppressed above the I_c, which causes a sudden increase of V in the figure 2(a). While below I_c, the $I − V$ curves overlap with each other exhibiting an abnormal parabolic-like behavior. Such a parabolic-like voltage behavior should be closely related to the electronic properties of junction between the graphene and single-unit-cell Bi2212
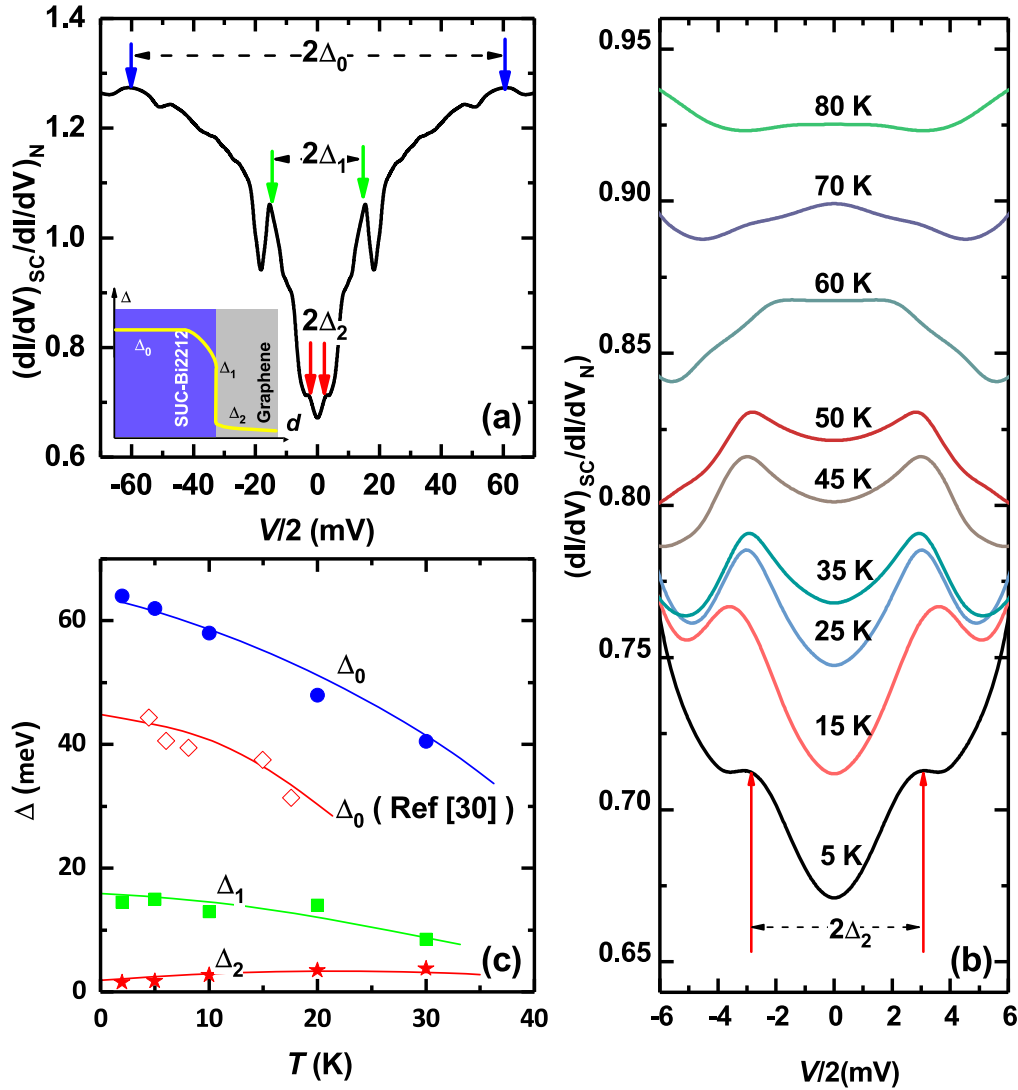
Figure 3. (a) Differential conductance $(dI/dV)_s$ at $T = 5$ K normalized by $(dI/dV)_N$ at 90 K for graphene/single-unit-cell Bi2212 heterostructures. There are three gaps Δ_0 (the blue), Δ_1 (the green), Δ_2 (the red) which can be identified as the intrinsic gap of single-unit-cell Bi2212, reduced gap at interface and induced gap in graphene, respectively. The inset: schematic drawing of the superconducting gaps in proximity effect. (b) The enlarge plot of Δ_2 from (a) at $5 \leqslant T \leqslant 80$ K. (c) T dependence of Δ_0 (blue circles), Δ_1 (green squares) and Δ_2 (red stars). The red diamonds is the Δ_0 from [39]. The solid lines are a guide to the eye.

heterostructure, since either Bi2212 or graphene would not show such a behavior individually. Actually a significant nonlinear $I - V$ behavior was previously observed in vertical graphene heterostructures called as graphene tunnel field-effect transistors (FETs) [33–36]. In these, the tunnel current is controlled by Fermi energy (E_F) of monolayer graphene, which is sensitive to the bias voltage owing to the low density of states and one-atom thickness of graphene [33]. Such an electric field also acts on the monolayer graphene in the geometry configuration of the inset to figure 2(b), when the single-unit-cell Bi2212 loses resistance at the super-conducting state.

In order to further clarify the nature of the parabolic-like voltage behavior, we plot the V^2 v.s. I in the figure 2(b), where the dash line is the linear fitting curve. It is shown that $V^2 \propto I$ when the I is larger than about 0.27 mA but deviates downward from the linear curve at $I < 0.27$ mA. This

behavior can be understood as the result of the Fermi energy of graphene tuned by the voltage applied on the junction, which is half of the drain voltage since there is no net electric field inside the superconducting single-unit-cell Bi2212 as shown in the inset to figure 2(b). In the limit of high bias voltage, superconducting effects become negligible and the differential tunneling conductance dI/dV is the product of electronic density of states (DOS) on both sides of the junction and tunneling probability [37, 38] as in the normal material junction. In particular to the graphene junction, the density of states of graphene (DOS_g) plays a major role in the tunability of tunneling dI/dV for its high sensitive to the bias electric field [33]. Thus the dI/dV is roughly proportional to DOS_g when the Fermi level of graphene fall outside the superconducting gap of Bi2212. The obtained relation of $V^2 \propto I$ therefore suggests $dI/dV \propto DOS_g \propto V$, which is consistent with the linear DOS of the Dirac cone of graphene

[2]. We note that such a characteristic could serve as a simple criteria for the Dirac-like band structure from similar transport measurements.

On the other hand, the E_F of graphene falls in between of single-unit-cell Bi2212 superconducting gap in the low bias voltage, at which Andreev reflection mechanism [22] is expected to occur at the interface between graphene and BSCCO. Different from the tunneling process discussed above, Andreev reflection involves in the process that the normal current is converted to a supercurrent. Andreev reflection states that an electron at energies less than the superconducting energy gap is converted to a hole with opposite spin and velocity but equal momentum, which thus produces an extra current through the junction. Consequently, it leads to the downward deviation from $V^2 \propto I$ as in figure 2(b).

For study of this superconducting proximity effect on graphene, we investigate the differential resistance dV/dI under different DC bias. Figure 3(a) shows the normalized differential conductances $(dI/dV)_{SC}/(dI/dV)_N$ as a function of $V/2$ for the graphene/single-unit-cell Bi2212 heterostructure at $T = 5\,$K, where $(dI/dV)_N$ is the differential conductance at 90 K. It is worth noting that the applied voltage on the junction is one half of the drain-source voltage V. This differential conductance spectrum consists of three sets of conductance peaks, which are located in at about Δ_0 (blue arrows), Δ_1 (green arrows) and Δ_2 (red arrows), respectively. Such a differential conductance spectrum was previously observed in the Bi_2Se_3/Bi2212 van der Waals junctions and was interpreted as the result of the leakage of the superconducting order parameter into a normal region [39, 40]. In this picture, the intrinsic superconducting gap Δ_0 is depressed at the interface while a proximity-induced superconducting gap Δ_2 is present at the normal region as shown in the inset to 3(a). It thus means that a superconductivity might be induced in graphene even by single-unit-cell thick Bi2212 according to figure 3(a). It is worth noting that superconducting correlation penetrates a distance $\xi \equiv \sqrt{\hbar D/\epsilon}$ into a normal metal, where D is diffusion constant and ϵ is the energy relative to the maximum of temperature $k_B T$ or bias voltage eV [41–45]. For a graphene (0.3 nm thickness) adjacent to a superconductor, the superconductivity could, in principle, be fully induced in the graphene at low temperature and at zero bias. Meanwhile, an induced gap is expected to be observed in the proximity-induced superconducting graphene.

To clarify the possible proximity-induced superconductivity in graphene, we enlarge the Δ_2 as shown in the figure 3(b). It is worth noting that the gap size of $\Delta_2 \approx 3\,$meV at the lowest temperature has the same order as the previously observed proximity-induced p–wave superconductivity in monolayer graphene by electron-doped cuprate superconductor PCCO [19]. In contrast to the graphene/PCCO heterostructure, figure 3(b) shows that the Δ_2 in graphene is observable even up to 60K. It implies that the high-temperature superconductivity might survive even at one-atom thickness. The evolutions of Δ_0, Δ_1 and Δ_2 with temperature (T) for single-unit-cell Bi2212 are summarized in

figure 3(c). It is found that the Δ_0 of single-unit-cell Bi2212 (solid blue) is larger than the reported intrinsic superconducting gap of bulk Bi2212 (hollow red) [39]. The enlarged Δ_0 in single-unit-cell Bi2212 is similar to the iron-based superconductors FeSe where the single layer FeSe has a much larger superconducting gap than the bulk FeSe [46]. However, in contrast to a significant increase in T_c of FeSe, the T_c of single-unit-cell Bi2212 is almost the same as bulk Bi2212, which thus calls for a further study by a scanning tunneling microscope (STM).

4. Conclusion

In summary, we fabricate the monolayer graphene/single-unit-cell Bi2212 van der Waals heterostructure. We found the superconductivity of single-unit-cell Bi2212 is present below 86 K along with a small subgap open up to 60 K, which might originate from the proximity-induced superconductivity in graphene. Our results provide a new insight into the induced superconductivity in two-dimensional Dirac fermion systems.

ORCID iDs

Hong Xiao ⓘ https://orcid.org/0000-0001-8859-9967
T Hu ⓘ https://orcid.org/0000-0003-0338-9632

References

[1] Novoselov K S, Geim A K, Morozov S V, Jiang D, Zhang Y, Dubonos S V, Grigorieva I V and Firsov A A 2004 *Science* **306** 666–9
[2] Novoselov K, Jiang D, Schedin F, Booth T, Khotkevich V, Morozov S and Geim A 2005 *Proc. Natl Acad. Sci.* **102** 10451–3
[3] Zhang Y, Tan Y W, Stormer H L and Kim P 2005 *Nature* **438** 201
[4] Stankovich S, Dikin D A, Dommett G H, Kohlhaas K M, Zimney E J, Stach E A, Piner R D, Nguyen S T and Ruoff R S 2006 *Nature* **442** 282
[5] Geim A K and Novoselov K S 2009 The rise of graphene *Nanoscience and Technology: A Collection of Reviews from Nature Journals* ed P Rodgers (Singapore: World Scientific) pp 11–9
[6] Neto A C, Guinea F, Peres N M, Novoselov K S and Geim A K 2009 *Rev. Mod. Phys.* **81** 109
[7] Cao Y *et al* 2018 *Nature* **556** 80
[8] Heersche H B 2007 *Nature (London)* **446** 56
[9] Du X, Skachko I and Andrei E Y 2008 *Phys. Rev.* B **77** 184507
[10] Komatsu K, Li C, Autier-Laurent S, Bouchiat H and Gueron S 2012 *Phys. Rev.* B **86** 115412
[11] Calado V 2015 *Nat. Nanotechnol.* **10** 761

[12] Shalom M B, Zhu M and Falko V 2016 *Nat. Phys.* **12** 318
[13] Kessler B, Girit C, Zettl A and Bouchiat V 2010 *Phys. Rev. Lett.* **104** 047001
[14] Allain A and Han Z 2012 *Nat. Mater.* **11** 590
[15] Han Z, Allain A, Arjmandi-Tash H, Tikhonov K, FeigelMan M, Sacepe B and Bouchiat V 2014 *Nat. Phys.* **10** 380
[16] Sun Y, Xiao H, Zhang M, Xue Z, Mei Y, Xie X, Hu T, Di Z and Wang X 2018 *Nat. Commun.* **9** 2159
[17] Tonnoir C, Kimouche A, Coraux J, Magaud L, Delsol B, Gilles B and Chapelier C 2013 *Phys. Rev. Lett.* **111** 246805
[18] Jiang D *et al* 2014 *Nat. Commun.* **5** 5708
[19] Di Bernardo A 2017 *Nat. Commun.* **8** 14024
[20] Beenakker C 2006 *Phys. Rev. Lett.* **97** 067007
[21] Beenakker C 2008 *Rev. Mod. Phys.* **80** 1337
[22] Andreev A 1965 *Sov. Phys. JETP* **20** 1490
[23] Perconte D *et al* 2018 *Nat. Phys.* **14** 25
[24] Haigh S, Gholinia A, Jalil R, Romani S, Britnell L, Elias D, Novoselov K, Ponomarenko L, Geim A and Gorbachev R 2012 *Nat. Mater.* **11** 764
[25] Wu T *et al* 2016 *Nat. Mater.* **15** 43
[26] Charlat P, Courtois H, Gandit P, Mailly D, Volkov A and Pannetier B 1996 *Phys. Rev. Lett.* **77** 4950
[27] Courtois H, Charlat P, Gandit P, Mailly D and Pannetier B 1999 *J. Low Temp. Phys.* **116** 187–213
[28] Poirier W, Mailly D and Sanquer M 1997 *Phys. Rev. Lett.* **79** 2105

[29] Den Hartog S, Kapteyn C, Van Wees B, Klapwijk T and Borghs G 1996 *Phys. Rev. Lett.* **77** 4954
[30] Golubov A A, Wilhelm F and Zaikin A 1997 *Phys. Rev.* B **55** 1123
[31] Nazarov Y V and Stoof T 1996 *Phys. Rev. Lett.* **76** 823
[32] Kulik I O and Ellialtiogammalu R 2012 *Quantum Mesoscopic Phenomena and Mesoscopic Devices in Microelectronics* vol 559 (Dordrecht: Springer)
[33] Britnell L *et al* 2012 *Science* **335** 947–50
[34] Georgiou T *et al* 2013 *Nat. Nanotechnol.* **8** 100
[35] Lee G H *et al* 2013 *ACS Nano* **7** 7931–6
[36] Moriya R, Yamaguchi T, Inoue Y, Morikawa S, Sata Y, Masubuchi S and Machida T 2014 *Appl. Phys. Lett.* **105** 083119
[37] Bardeen J 1961 *Phys. Rev. Lett.* **6** 57
[38] Tersoff J 1985 *Phys. Rev.* B **31** 805
[39] Zareapour P *et al* 2012 *Nat. Commun.* **3** 1056
[40] Li A J, Zhu X, Stewart G and Hebard A F 2017 *Sci. Rep.* **7** 4639
[41] Volkov A F, Zaitsev A V and Klapwijk T M 1993 *Physica* C **210** 21–34
[42] Volkov A F and Zaitsev A V 1996 *Phys. Rev.* B **53** 9267
[43] Zaitsev A V 1990 *JETP Lett* **51** 41
[44] Zaitsev A V 1994 *Phys. Lett.* A **194** 315–22
[45] Zhou F, Spivak B and Zyuzin A 1995 *Phys. Rev.* B **52** 4467
[46] Qing-Yan W *et al* 2012 *Chin. Phys. Lett.* **29** 037402